LETTER

Holographically Defined TiO_2 Electrodes for Dye-Sensitized Solar Cells

Woo-Min Jin,[†] Ju-Hwan Shin,[†] Chang-Yeol Cho,[†] Ji-Hwan Kang,[†] Jong Hyeok Park,[‡] and Jun Hyuk Moon*,[†]

Department of Chemical and Biomolecular Engineering, Sogang University, 1 Sinsu-dong Mapo-gu, Seoul, Republic of Korea, Department of Chemical Engineering, Sungkyunkwan University, Suwon 440-746, Republic of Korea

ABSTRACT We describe a multibeam interference lithography for creating 3D polymeric porous structures. The coating of a TiO_2 shell and subsequent removal of the template produce holographically defined TiO_2 (h-TiO_2) electrodes. We analyze the morphological features of the h-TiO_2 electrodes and consider their applicability to dye-sensitized solar cells (DSSCs). Specifically, the performance of the h-TiO_2 electrode was evaluated by comparison with a macroporous TiO_2 electrode produced from colloidal crystals. The h-TiO_2 structure possesses a larger specific area than the inverted colloidal crystals because of a bicontinuous air network with the TiO_2 shell. Consequently, the h-TiO_2 electrode can produce a 30% higher photogenerated electron current.

KEYWORDS: holographic lithography • solar cells

INTRODUCTION

Dye-sensitized solar cells (DSSCs) are attractive as potential next-generation photovoltaic devices because of their simple and low-cost fabrication (1). Intensive research efforts have been made to improve each component of DSSCs, including the electrolyte solution (2), the sensitizer dye (3), and the electrode material (4), as well as to optimize the fabrication techniques (5, 6). In DSSCs, light is harvested by a TiO_2 layer. This layer acts as a substrate on which the dye molecules adsorb; it transfers the photogenerated electrons and serves as a diffusion pathway for ions in the electrolyte solution. Therefore, the engineering of TiO_2 electrodes with regard to properties such as nanostructure, crystalline morphology, and surface properties is a crucial aspect of efforts to enhance the photoconversion efficiency (7−10). Typical TiO_2 electrodes are formed by depositing nanocrystalline TiO_2 (nc-TiO_2) particles with diameters of 10−20 nm onto a transparent conducting substrate. The nanocrystalline TiO_2 electrodes possess large surface areas due to numerous mesopores among the particles. Thus, this kind of mesoporous film enables high-density loading of dye molecules, resulting in a large photocurrent density.

In addition to forming mesoscale pores in TiO_2 electrodes, several recent approaches have taken advantage of macroscale morphologies with typical feature sizes on the order of 100 nm. For example, macropores have been introduced into nc-TiO_2 films as a small portion of the electrode; whole, ordered macropores have also been used as the electrode itself (11−14). Although the introduction of macroscale morphologies decreases the surface area accordingly, the electrolyte solution can be easily infiltrated and the mass transport of electrolyte ions can be enhanced through extensive open-pore networks (14−16). Therefore, this type of macroporous electrode may be important for solid or quasi-solid electrolytes, which possess a high viscosity and contain relatively large molecules or particles (17).

Here, we introduce a top-down holographic lithography technique for fabricating ordered macroporous TiO_2 electrodes (h-TiO_2) for use in DSSCs. The previous result on the optimization of macropore size shows that larger pores about 1 μm shows higher efficiency due to enhanced adhesion between their inverted structure and the substrate (14). The morphological advantages and performance of DSSCs containing h-TiO_2 were investigated by comparison with inverted colloidal crystal macroporous electrodes. The first accomplishment of this work lies in the application of holographic lithography to the design of macroporous TiO_2 electrodes for DSSCs. Previously, holographic lithography has been applied to fabricating polymeric sacrificial templates for TiO_2 photonic crystals (18). Control of the volume fraction of TiO_2 is important in controlling the photonic bandgap properties. In this regard, deposition of TiO_2 with completely filled pores is favored for increasing the photonic bandgaps (19, 20). However, in electrode applications, the surface area of the TiO_2 structure should be carefully controlled instead. In our study, we reveal that incompletely filled TiO_2 with a shell morphology has an advantage because it can offer a larger surface area than the completely filled structures do.

The second accomplishment is that our h-TiO_2 electrode possesses unique advantages over the inverted colloidal crystal electrode, which has recently been suggested as a novel method for producing macroporous electrodes for

* Corresponding author. E-mail: junhyuk@sogang.ac.kr.
Received for review August 2, 2010 and accepted October 18, 2010
[†] Sogang University.
[‡] Sungkyunkwan University.
DOI: 10.1021/am100681f

Published on Web 10/27/2010

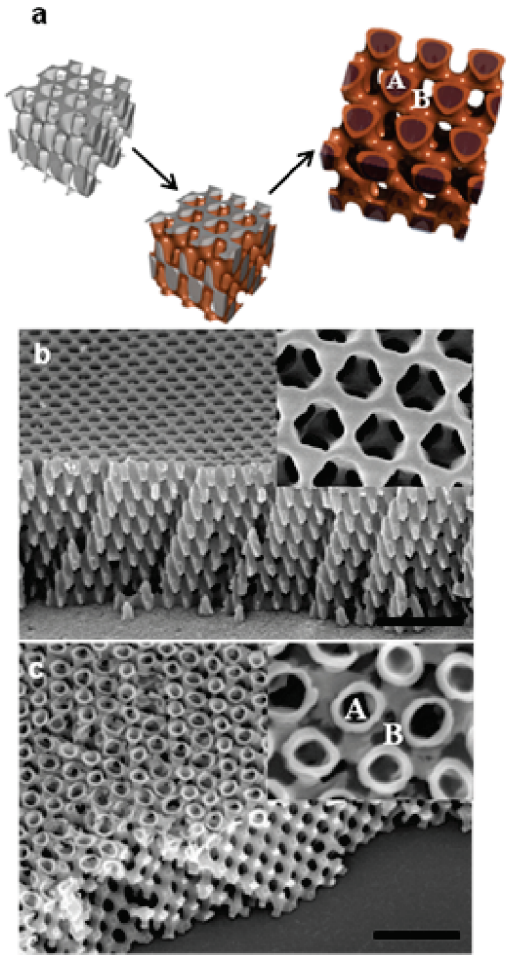

FIGURE 1. (a) Fabrication of an inverted TiO_2 structure from the SU-8 template: coating of the TiO_2 shell and subsequent removal of the template. (b) SEM image of macroporous SU-8 patterns on FTO and an inset image of the magnified surface. (c) SEM image of inverted TiO_2 patterns and an inset image of the magnified surface. A and B indicate triply periodic, bicontinuous air networks formed after removal of the SU-8 template and after coating with TiO_2. (The scale bars for b and c indicate 3 μm.)

DSSCs (14). Here, the performance of h-TiO_2 electrodes for DSSCs was compared with the performance of one from a colloidal crystal template. Photovoltaic measurements showed that the larger specific area of h-TiO_2 resulted in 30% more photocurrent density as compared with an inverted colloidal crystal electrode of the same volume and therefore had a higher photoconversion efficiency. Although the absolute efficiency of DSSCs with h-TiO_2 is still too low to compete with a conventional nc-TiO_2 electrode, optimization of the electrode thickness and the introduction of a mesoporous TiO_2 shell can further enhance the efficiency (8). Again, we stress that this type of macroporous electrode may be important and is more appropriate for use with solid-like electrolytes because of its well-connected and size-controllable pores, features that cannot be reproduced in conventional mesoporous TiO_2 electrodes.

RESULTS AND DISCUSSION

The following is a brief description of the fabrication process for h-TiO_2 electrodes for DSSCs (see Figure 1a): The four-beam constructed interference patterns with face-centered cubic(FCC) symmetry, which was transferred to SU-8 photoresist. The detailed lithographic conditions are described elsewhere (21). It is noteworthy that a TiO_2 shell was deposited on the surface of the SU-8 by spin-coating of dilute $TiCl_4$ precursor solution. The macroporous h-TiO_2 structure was obtained after removal of the SU-8 template by calcination.

Figure 1b shows scanning electron microscopy (SEM) images of FCC SU-8 structures on the fluorine doped tin oxide (FTO) substrate formed by this holographic lithography technique. The thickness of the patterned SU-8 film was 4.8 $\pm$ 0.2 μm. The SU-8 structure possessed intertwined SU-8/macropore networks in all three dimensions, that is, the structure was triply periodic bicontinuous. The triply periodic SU-8 structure possessed a connected cylindrical motif of air cavities in an FCC lattice, and the spacings between motifs in the (111) plane and (111) layers were measured to be 0.71 and 0.74 μm, respectively. Figure 1c shows an SEM image of the h-TiO_2 structure. The thickness of the h-TiO_2 layer was reduced to 3.7 $\pm$ 0.3 μm after calcination, and the spacings between motifs in the (111) plane and (111) layers were 0.70 and 0.59 μm, respectively. Therefore, the pattern shrank mainly in the same direction as the substrate, and the shrinkage was estimated to be about 20%. The TiO_2 shell with a 70−90 nm thickness exhibited the anatase phase (not shown).

The surface area of the TiO_2 structure was investigated because the amount of sensitizing dye molecules adsorbed was directly proportional to the surface area of the TiO_2 film. Thus, a larger surface area is favorable for producing photogenerated electrons. Specifically, we compared the h-TiO_2 electrode with the inverted FCC colloidal crystal electrode shown in Figure S1 in the Supporting Information. The surface areas of the two samples can be compared in terms of the specific area (surface area per unit sample volume). In h-TiO_2, as shown in Figure 1c, two triply continuous open pores were created: one was created by removal of the SU-8 (A in Figure 1a,c), and the other was composed of unfilled pores outside the h-TiO_2 shell (B in Figure 1a,c). The specific area of the FCC holographic patterns has a range of 3.36−3.84 m^{-1} depending on their volume fraction in the range of 0.25−0.75, which can be controlled by lithographic conditions (22). For a volume fraction of about 0.5 in our patterns, the specific area of holographic patterns can be calculated to be 3.84 m^{-1}, assuming that the morphology is similar to the diamond D structure (22). The specific area of the h-TiO_2 structure was double this value, around 7.68 m^{-1}, because both sides of the h-TiO_2 shell were available for dye adsorption.

Meanwhile, when using the FCC colloidal crystal template, the deposition of TiO_2 under the same condition filled most of the air cavities of the colloidal crystal (B in Figure S1b), and the areas outside the TiO_2 shell might not be accessible for dye adsorption, which is distinct from the h-TiO_2 structure. This is due to lower volume fraction of air cavities in colloidal crystals, fixed at 0.24. The specific area of FCC colloidal crystals is 6.28 m^{-1} (total surface area per unit volume, $4 \times 4\pi r^2$ m^2 m^{-3}, where $r = \sqrt{2}/4$ for closely

Table 1. Photovoltaic Parameters of Dye-Sensitized Solar Cells Containing h-TiO_2 or Inverted Colloidal Crystal Electrodes

			photovoltaic parameters			
sample	estimated specific area (m^2 m^{-3})	adsorbed dye (mmol cm^{-3})	V_{oc} (V)	J_{sc} (mA cm^{-2})	FF (%)	η (%)
h-TiO_2	7.68	0.041 ± 0.05	0.82 ± 0.03	6.1 ± 0.3	58 ± 2	2.9 ± 0.3
inverted colloidal crystals	6.28	0.035 ± 0.04	0.85 ± 0.01	4.7 ± 0.2	62 ± 1	2.6 ± 0.1

packed spheres). Because of the complete filling, the specific area of the inverted colloidal crystals accounts only for the area that was in contact with colloidal crystals and thus might be similar to that of colloidal crystals, 6.28 m^{-1}. Therefore, a morphological analysis in terms of specific area showed that the area of h-TiO_2 is about 22% (7.68 m^{-1}/6.28 m^{-1}) larger than that of the inverted colloidal crystals.

Meanwhile, a relative comparison of the surface area of the TiO_2 films can be estimated by an experimental measurement of the amount of dye molecules adsorbed. The concentration of dye molecules detached from both TiO_2 electrodes was measured spectrophotometrically. The quantity of adsorbed molecules per unit volume for the h-TiO_2 structure was 0.041 ± 0.05 mmol/cm^3, compared with 0.035 ± 0.04 mmol/cm^3 for the inverted colloidal crystals (Table 1). The loading of dye molecules per unit volume on the h-TiO_2 structure was about 17% higher than that on the inverted colloidal crystal, which is similar to the 22% measured from the estimated specific areas.

The h-TiO_2 electrode was sensitized with dye molecules and then assembled with a Pt-coated counter electrode. The gap between electrodes was filled with a redox electrolyte solution containing I^-/I^{3-} ion pairs. The photocurrent and voltage of the DSSC containing were measured using a sourcemeter under a simulated solar light. The performance of the h-TiO_2 electrode was evaluated by comparison with a macroporous TiO_2 electrode produced from colloidal crystals. Table 1 lists the photovoltaic parameters, including the short-circuit photocurrent density (J_{sc}), the open-circuit voltage (V_{oc}), and the fill factor (FF), for both the h-TiO_2 and inverted colloidal crystal electrodes. Figure 2 shows a representative photocurrent density−voltage curves. The V_{oc} values of both electrodes were higher than that of typical nc-TiO_2 electrodes, which have a V_{oc} of about 0.75−0.78 V. This may be partially related to the thinness of the electrode (4 μm) and the precoated TiO_2 blocking layer under these electrodes

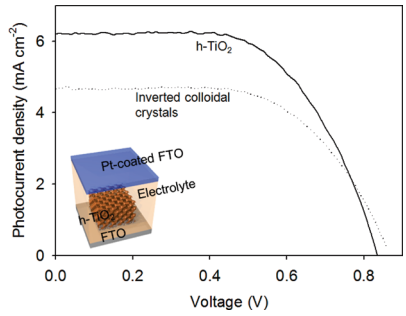

FIGURE 2. Representative photocurrent density−voltage curves for DSSCs containing an h-TiO_2 electrode or an inverted colloidal crystal electrode. An inset camera image of a DSSC containing an h-TiO_2 electrode.

(10). Moreover, the FF of both electrodes were relatively low compared to that of nc-TiO_2 electrodes due to the high resistance between porous TiO_2 and the substrate (23).

The overall conversion efficiency (η) was calculated using the equation $\eta = J_{sc} \times V_{oc} \times$ FF/P, where P is the power density of the incident light (100 mW/cm^2). The DSSC with the h-TiO_2 electrode exhibited a higher efficiency than the device based on the inverted colloidal crystal electrode. This is attributed to the higher J_{sc} of the h-TiO_2: as shown in Table 1, the J_{sc} of the h-TiO_2 electrode was 6.1 ± 0.3 mA/cm^2, around 30% higher than the value of 4.7 ± 0.2 mA/cm^2 for the inverted colloidal crystals. Because both the h-TiO_2 and inverted colloidal crystal electrodes were prepared under the same conditions and both electrodes showed a similar transmittance (only a 2−3% difference, see Figure 2S in the Supporting Information), the difference in the J_{sc} values between samples with the same thickness can be attributed mainly to the amount of adsorbed dye molecules per sample volume. We believe that, considering the errors involved in the aforementioned estimation and the photovoltaic measurement, the 29% higher J_{sc} of the h-TiO_2 is supported by the previous results of 17% and 22% higher specific area. Therefore, the higher loading of dye molecules per sample volume of the h-TiO_2 electrodes leads to a higher photocurrent density in DSSCs.

Meanwhile, we compared the efficiency of h-TiO_2 to that of a conventional nanocrystalline TiO_2 electrode. Under our experimental conditions, the DSSC efficiency for a conventional TiO_2 electrode (Dyesol, 18NRT) with a 4-μm thickness was 4.7%, as calculated from a short-circuit photocurrent density (J_{sc}) of 10 mA/cm^2, an open-circuit voltage (V_{oc}) of 0.72 V, and a fill factor (FF) of 65%. This efficiency is lower than those of previous results by ~25% (24). As compared to the results for the nc-TiO_2 electrodes, the lower efficiency of the h-TiO_2 electrodes was due to a lower J_{sc} and FF, by 45 and 11%, respectively. The lower J_{sc} can be attributed to the lower specific area of h-TiO_2 due to the larger pore size. The lower FF may be attributable to a higher contact resistance between the TiO_2 and the FTO substrate.

CONCLUSIONS

To summarize, we introduced a new type of macroporous electrode for DSSCs that is defined by 3D holographic lithography. A triply periodic, bicontinuous network with a TiO_2 shell interface was fabricated by using a holographically designed template. Due to the formation of an additional continuous air network in the h-TiO_2 template, the h-TiO_2 shows a larger specific area than the inverted colloidal crystal electrode. Consequently, the h-TiO_2 electrode provides a larger area for dye adsorption per sample volume and thus

can produce a higher photogenerated electron current density (by about 30%) and a concurrently higher DSSC efficiency. Although the absolute efficiency of the DSSCs in this work is low because introducing macropores decreased the surface area, we believe that it is still possible to enhance the efficiency by optimizing the TiO_2 post-treatment or electrode thickness (25, 26). For example, the thickness of the electrode was required to be controlled because as the thickness increased, the harvesting of photogenerated electrons increased due to a higher density of adsorbed dyes per unit surface area (26). However, the increased surface area also provided additional interfacial area for electron recombination with the electrolytes in solution. We are currently investigating the application of h-TiO_2 electrodes in conjunction with gel electrolytes. This type of macroporous electrode may have more compatible with solid or quasi-solid electrolytes, which possess a high viscosity and contain large polymeric molecules or particles (17).

EXPERIMENTAL SECTION

Fabrication of h-TiO_2 via Holographic Lithography. The FTO substrate was pretreated by soaking in 0.1 M $TiCl_4$ aqueous solution at 70 °C for 30 min. The SU-8 photoresist was spin-coated on the pretreated FTO. The SU-8 photoresist was prepared by dissolving SU-8 resin and a cationic photoinitiator (triarylsulfonium hexafluorophosphate salts, Sigma-Aldrich) in γ-butyrolactone (Sigma-Aldrich). An 325 nm He−Cd laser beam (50 mW, Kimmon) was exposed onto the top-cut fused multifaceted silica prism to form an interference pattern (18, 21). After postexposure baking at 55 °C and subsequent development, a macroporous SU-8 structure was obtained. The sol−gel precursor solution of 1.0 M $TiCl_4$ (Sigma-Aldrich) in ethanol and DI water was spin-coated at 2000 rpm for several seconds. The samples were then calcined in air at 450 °C for 1 h to burn away the polymeric SU-8, leaving behind a TiO_2 inverted structure.

Assembly of DSSC. The TiO_2 layer was immersed in a dye solution of 0.5 mM N719 dye (Dyesol) in anhydrous ethyl alcohol (99.9%, Sigma-Aldrich) for 20−30 h. Post-treatment of the TiO_2 layer was applied for 1 h prior to sensitization. The counter electrode was prepared by coating a 0.7 mM H_2PtCl_6 solution in anhydrous ethanol onto the FTO substrate. The TiO_2 electrode was assembled with the counter electrode, and the gap size between electrodes was controlled using a 25 μm thick polymeric film (Surlyn, Dupont). The electrolyte solution was injected into the gap. The redox couple/electrolyte solution was prepared by 0.7 M 1-butyl-3-methylimidazolium iodide (TCI), 0.03 M iodine (Yakuri), 0.1 M guanidinium thiocyanate (Wako), 0.5 M tert-butylpyridine (Aldrich) in a solution of acetonitrile (Aldrich) and valeronitrile (TCI) (85:15 v/v).

Characterization. In order to estimate the quantity of N719 dye molecules, the dye adsorbed on the TiO_2 electrode was detached in 0.1 M NaOH water/ethanol solution for several hours, and the absorption intensity of the dye solution was measured by UV−Vis spectrophotometer (JASCO V550). The photocurrent and voltage of the DSSC were measured using a sourcemeter (Keithly Instruments, model 2400) under a simulated solar light, produced by a 300 W Xe lamp (Oriel) and AM 1.5 filters. The intensity of the lamp was adjusted using a Si reference cell (BS-520, Bunko-Keiki) for 100 mW/cm^2. The transmission spectrum of the TiO_2 electrode was measured by the UV−vis spectrophotometer.

Acknowledgment. This work is supported by the National Research Foundation of Korea (KRF-2008-313-D00295, NRF-2010-0011024). The authors thank Dr. Sung-Gyu Park and Prof. Seung-Man Yang for helpful discussions. The Korea Basic Science Institute is also acknowledged for the measurement of SEM.

Supporting Information Available: SEM images and transmission spectra of colloidal crystals and TiO_2 inverted colloidal crystals (PDF). This material is available free of charge via the Internet at http://pubs.acs.org.

REFERENCES AND NOTES

(1) Oregan, B.; Gratzel, M. *Nature* **1991**, *353*, 737.
(2) Wu, J. J.; Chen, G. R.; Yang, H. H.; Ku, C. H.; Lai, J. Y. *Appl. Phys. Lett.* **2007**, *90*, 213109.
(3) Nazeeruddin, M. K.; Pechy, P.; Renouard, T.; Zakeeruddin, S. M.; Humphry-Baker, R.; Comte, P.; Liska, P.; Cevey, L.; Costa, E.; Shklover, V.; Spiccia, L.; Deacon, G. B.; Bignozzi, C. A.; Gratzel, M. *J. Am. Chem. Soc.* **2001**, *123*, 1613.
(4) Vomiero, A.; Concina, I.; Natile, M. M.; Comini, E.; Faglia, G.; Ferroni, M.; Kholmanov, I.; Sberveglieri, G. *Appl. Phys. Lett.* **2009**, *95*, 193104.
(5) Park, N. G.; Kim, K. M.; Kang, M. G.; Ryu, K. S.; Chang, S. H.; Shin, Y. J. *Adv. Mater.* **2005**, *17*, 2349.
(6) Liu, Y.; Wang, H.; Li, M.; Hong, R. J.; Ye, Q. H.; Zheng, J. M.; Shen, H. *Appl. Phys. Lett.* **2009**, *95*, 233505.
(7) Barbe, C. J.; Arendse, F.; Comte, P.; Jirousek, M.; Lenzmann, F.; Shklover, V.; Gratzel, M. *J. Am. Ceram. Soc.* **1997**, *80*, 3157.
(8) Chen, D. H.; Huang, F. Z.; Cheng, Y. B.; Caruso, R. A. *Adv. Mater.* **2009**, *21*, 2206.
(9) Qian, J. F.; Liu, P.; Xiao, Y.; Jiang, Y.; Cao, Y. L.; Ai, X. P.; Yang, H. X. *Adv. Mater.* **2009**, *21*, 3663.
(10) Koo, H. J.; Kim, Y. J.; Lee, Y. H.; Lee, W. I.; Kim, K.; Park, N. G. *Adv. Mater.* **2008**, *20*, 195.
(11) Ito, S.; Zakeeruddin, S. M.; Humphry-Baker, R.; Liska, P.; Charvet, R.; Comte, P.; Nazeeruddin, M. K.; Pechy, P.; Takata, M.; Miura, H.; Uchida, S.; Gratzel, M. *Adv. Mater.* **2006**, *18*, 1202.
(12) Lee, S. H. A.; Abrams, N. M.; Hoertz, P. G.; Barber, G. D.; Halaoui, L. I.; Mallouk, T. E. *J. Phys. Chem. B* **2008**, *112*, 14415.
(13) Hore, S.; Nitz, P.; Vetter, C.; Prahl, C.; Niggemann, M.; Kern, R. *Chem. Commun.* **2005**, 2011.
(14) Kwak, E. S.; Lee, W.; Park, N. G.; Kim, J.; Lee, H. *Adv. Funct. Mater.* **2009**, *19*, 1093.
(15) Kim, Y. J.; Lee, M. H.; Kim, H. J.; Lim, G.; Choi, Y. S.; Park, N. G.; Kim, K.; Lee, W. I. *Adv. Mater.* **2009**, *21*, 3668.
(16) Fujita, K.; Konishi, J.; Nakanishi, K.; Hirao, K. *Sci. Technol. Adv. Mater.* **2006**, *7*, 511.
(17) Somani, P. R.; Dionigi, C.; Murgia, M.; Palles, D.; Nozar, P.; Ruani, G. *Sol. Energy Mater. Sol. Cells* **2005**, *87*, 513.
(18) Moon, J. H.; Yang, S. *Chem. Rev.* **2010**, *110*, 547.
(19) Moon, J. H.; Xu, Y. G.; Dan, Y. P.; Yang, S. M.; Johnson, A. T.; Yang, S. *Adv. Mater.* **2007**, *19*, 1510.
(20) Xu, Y.; Zhu, X.; Dan, Y.; Moon, J. H.; Chen, V. W.; Johnson, A. T.; Perry, J. W.; Yang, S. *Chem. Mater.* **2008**, *20*, 1816.
(21) Park, S. G.; Lee, S. K.; Moon, J. H.; Yang, S. M. *Lab Chip* **2009**, *9*, 3144.
(22) Jung, Y.; Chu, K. T.; Torquato, S. *J. Comput. Phys.* **2007**, *223*, 711.
(23) Mor, G. K.; Varghese, O. K.; Paulose, M.; Shankar, K.; Grimes, C. A. *Sol. Energy Mater. Sol. Cells* **2006**, *90*, 2011.
(24) Wei, M. D.; Konishi, Y.; Zhou, H. S.; Yanagida, M.; Sugihara, H.; Arakawa, H. *J. Mater. Chem.* **2006**, *16*, 1287.
(25) Knorr, F. J.; Zhang, D.; McHale, J. L. *Langmuir* **2007**, *23*, 8686.
(26) Wang, Z. S.; Kawauchi, H.; Kashima, T.; Arakawa, H. *Coord. Chem. Rev.* **2004**, *248*, 1381.

AM100681F